HAL open science

Stochastic variability of large-scale oceanic flows above topography anomalies

Antoine Venaille, Julien Le Sommer, J.-M. Molines, B. Barnier

To cite this version:

Antoine Venaille, Julien Le Sommer, J.-M. Molines, B. Barnier. Stochastic variability of large-scale oceanic flows above topography anomalies. 2011. hal-00577907v1

HAL Id: hal-00577907

https://hal.science/hal-00577907v1

Preprint submitted on 18 Mar 2011 (v1), last revised 23 Jul 2011 (v2)

HAL is a multi-disciplinary open access archive for the deposit and dissemination of scientific research documents, whether they are published or not. The documents may come from teaching and research institutions in France or abroad, or from public or private research centers.

L'archive ouverte pluridisciplinaire **HAL**, est destinée au dépôt et à la diffusion de documents scientifiques de niveau recherche, publiés ou non, émanant des établissements d'enseignement et de recherche français ou étrangers, des laboratoires publics ou privés.

Stochastic variability of large-scale oceanic flows above topography anomalies

Antoine Venaille,* Julien Le Sommer, Jean-Marc Molines, and Bernard Barnier
LEGI/UJF/CNRS/INPG, Grenoble, France
(Dated: March 18, 2011)

Large-scale oceanic currents show large fluctuations at decadal, centennial and even millennial time scales [12]. Understanding the nature and the causes of this variability is a major challenge for climate predictions [4]. Here, we describe a new stochastic variability mechanism which is genuinely internal to the ocean, i.e. not due to fluctuations in atmospheric forcing. The key ingredient is the existence of closed contours of bottom topography surrounded by a stirring region of enhanced eddy activity. This configuration leads to the formation of a robust but highly variable vortex above the topography anomaly. The vortex dynamics integrates the white noise forcing of oceanic eddies into a red noise signal for the large scale volume transport of the vortex. The fluctuations of the transport of the Zapiola anticyclone ($\sim$ 100 Sv) in the Argentine basin are argued to be an example of such eddy-driven stochastic variability, on the basis of a 310 years long simulation of a comprehensive ocean model run driven by a repeated-year forcing.

Some properties of oceanic variability can result from the intrinsic, deterministic non-linear dynamics of oceanic flows [7]. For instance, this approach has been proven useful to interpret the different peaks arising at decadal time scales in time-series of the Gulf-Stream position [23]. Otherwise, the ubiquity of red noise signals in time series of various oceanic metrics is generally thought to result from the integration of white noise processes by the linearized dynamics [13]. Obviously, a source of noise is associated with the rapid fluctuations of atmospheric forcing, therefore leading to low frequency oceanic variability [9]. However, red noise signals have also been reported in ocean models forced by steady winds but with sufficient spatial resolution to simulate the "oceanic weather system", i.e. mesoscale eddies at scale from 30 to 300 km [2, 15]. The above studies suggest the existence of intrinsic, stochastic variability of large-scale oceanic currents.

The dynamics of eddy-driven barotropic (depth independent) flows above closed topography contours provides essential ingredients for supporting such stochastic variability. Let us consider for instance a barotropic flow above an axisymmetric topographic bump $h(r)$ surrounded by a "stirring" region, as sketched on figure 1-b. Here, stirring can be due to any mechanism outside the topography anomaly, generating disturbances in the flow field that propagate toward the topography anomaly. This situation is reminiscent of the large scale atmospheric circulation induced by mid-latitude stirring [29]. Simple arguments relying on Kelvin circulation theorem explain the formation of an anticyclonic flow above the closed topographic contours in the same way as westward flows are formed away from stirring regions in the atmosphere [14, 24]. Note that contrary to the atmospheric case, the stirring region is here located outside the topography anomaly. Therefore, the formation of a cyclonic flow pattern in the stirring region, equivalent to the mid-latitude eastward jet in the atmosphere, is not expected in this case.

Neglecting other forcing than stirring, and considering that dissipation occurs through bottom friction modeled as a linear drag with coefficient ω_b, the azimuthal average of the volume transport $\mathcal{T}$ between the center ($r = 0$) and the boundary ($r = L_h$) of the bump can be shown to obey a simple equation (see methods for more details):

$$\frac{d\mathcal{T}}{dt} = \eta_{eddy} - \omega_b \mathcal{T}, \tag{1}$$

where $\eta_{eddy}(t)$ is the vertically and azimuthally integrated eddy momentum flux through the boundary $r = L_h$. In the absence of direct external forcing, eddy fluxes tend to reduce large scale potential vorticity gradients, therefore driving anticyclonic flow above topographic bumps [20]. One expect then that time-mean of the eddy term η_{eddy} is positive (resp. negative) in the case of a positive (resp. negative) topography anomaly. If η_{eddy} were time independent, the vortex would reach a stationary state and its transport would be inversely proportional to bottom friction [6]. However, stirring is more generally time varying, and so is the driving term η_{eddy}. In particular, the eddy term η_{eddies} could possibly vary depending on the anticyclone transport $\mathcal{T}$, thus allowing complex feedbacks as in the case of the atmosphere [17]. Assuming here that such feedbacks are negligible, and modelling the eddy term $\eta_{eddy}(t)$ as a constant plus a gaussian white noise, the transport satisfies a Langevin equation. Transport time series are then instances of an auto-regressive process of order one [13, 26]. For frequency ω higher than the cutt-off frequency ω_b set by bottom friction, the transport power spectrum $|\widetilde{\mathcal{T}}(\omega)|^2 = |\widetilde{\eta}_{eddy}|^2(\omega^2 + \omega_b^2)^{-1}$ is a red noise. This shows that oceanic eddies can drive the formation and the low frequency variability of anticyclonic flows above topographic bumps.

*Current Affiliation: GFDL, AOS, Princeton University, Forrestal campus 08540 Princeton NJ US; Electronic address: venaille@princeton.edu

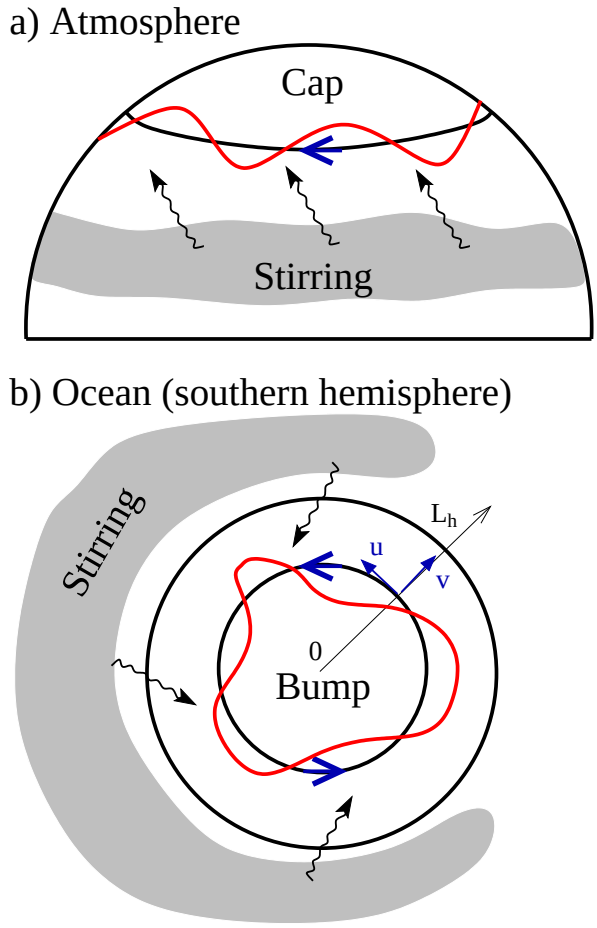

FIG. 1: **Large scale flows driven by eddies in presence of a mean gradient of potential vorticity f/h. a)** Case of mid-latitude atmospheric circulation: the potential vorticity gradient is due to variations of the Coriolis parameter f with latitude (beta effect). Arrows represent Rossby waves that propagate away from the stirring region and imply the formation of a westward flow outside the stirring region and an eastward flow in the stirring region [24, adapted from figures 12.2 and 12.3]. **b)** Case of oceanic flows above a topographic bump of typical length $L_h = 600$ km: the potential vorticity gradient is due to variations of depth h.

We argue that the above mechanism is responsible for the massive fluctuations in transport time series of the Zapiola Anticyclone [21]. The Zapiola anticyclone is a strong and robust anticyclonic vortex above a sedimentary bump (the Zapiola drift), located in the Argentine basin, around ($45°S$, $45°W$), see figure 2.

This bump is characterized by shoaling bottom topography rising by $\sim$ 800 m over a distance of $\sim$ 400 km. The anticyclone appears as a local maximum in sea surface height as shown in figure 2-a. Typical velocities of the anticyclone are about 0.1 $m.s^{-1}$ over the whole vertical water column ($\sim$ 5000 m depth). The associated transport is of the order of 100 Sv ($= 10^6\ m^3.s^{-1}$) which is comparable with other major oceanic currents including the Gulf-Stream. Remarkably, the Zapiola anticyclone is surrounded by one of the most eddying region of the global ocean, namely the confluence between the Nord-Brazil current and the Malvinas current (see figure 2-b). Perhaps surprisingly, the Zapiola anticyclone has only been discovered rather lately, and almost simultaneously with in situ measurement [22, 27], numerical ocean models [5], and in theoretical studies [6]. Also striking is the strong interannual variability of the Zapiola anticyclone transport which has recently been reported from 15 years of altimetric measurements [21]. High resolution data syntheses also suggest the dominance of interior ocean dynamics as opposed to atmospheric forcing in determining the variability of the Zapiola anticyclone [25]. But the strong variability of the Zapiola anticyclone transport remains unexplained.

Here, we report strong interannual fluctuations of the Zapiola anticyclone transport in a 310 year long simulation of a comprehensive ocean model run under a repeated-year forcing (see methods for details on the ocean model and diagnostics). Figure 3-a,b show these strong fluctuations of transport over the last 10 years of the simulation and the associated power-spectrum computed over the first 300 years of the simulation. The model being forced by repeated-year atmospheric fields, the wind forcing is practically identical every year. Therefore, in the model, interannual fluctuations of Zapiola anticyclone transport can only be due to intrinsic ocean dynamics.

A comparison of time series of transport $\mathcal{T}$ and the time series of the eddy momentum flux η_{eddy} is performed over the last 10 years of the simulation, see figure 3. Remarkably, fluctuations of the eddy momentum flux are essentially white at frequency ω lower than $\omega_{topo} \sim (20\ \text{days})^{-1}$ (figure 3-c) . This correlation time scale corresponds to the period of a barotropic dipole rotating around the Zapiola drift [11, 16], and interpreted either as a topographic Rossby wave [11], or as the superposition of Rossby basin modes [28]. As expected from equation (1), for frequency ω lower than ω_{topo}, the transport power spectra of figures 3-a and 3-c are well fitted by the function $a(\omega^2 + \omega_b^2)^{-1}$, where the cut-off frequency ω_b is estimated by evaluating the ratio between time-mean transport and time-mean eddy momentum flux $\langle \eta_{eddy} \rangle / \langle T \rangle \sim (15\ \text{months})^{-1}$, and where the coefficient a is the low-frequency asymptotic value of the transport power spectrum. Strikingly, the value of the cut-off frequency ω_b estimated from the transport and eddy momentum flux time series is of similar magnitude as the effective bottom friction coefficient used in the model (estimated at about $(14\ \text{month})^{-1}$, see methods). The above diagnostics support the idea that the red noise spectrum of the Zapiola anticyclone transport time series (at seasonal to interannual time scale, see figure 3-a) results from the integration by the dynamics of the eddy momentum flux fluctuations at the boundary of the anticyclone.

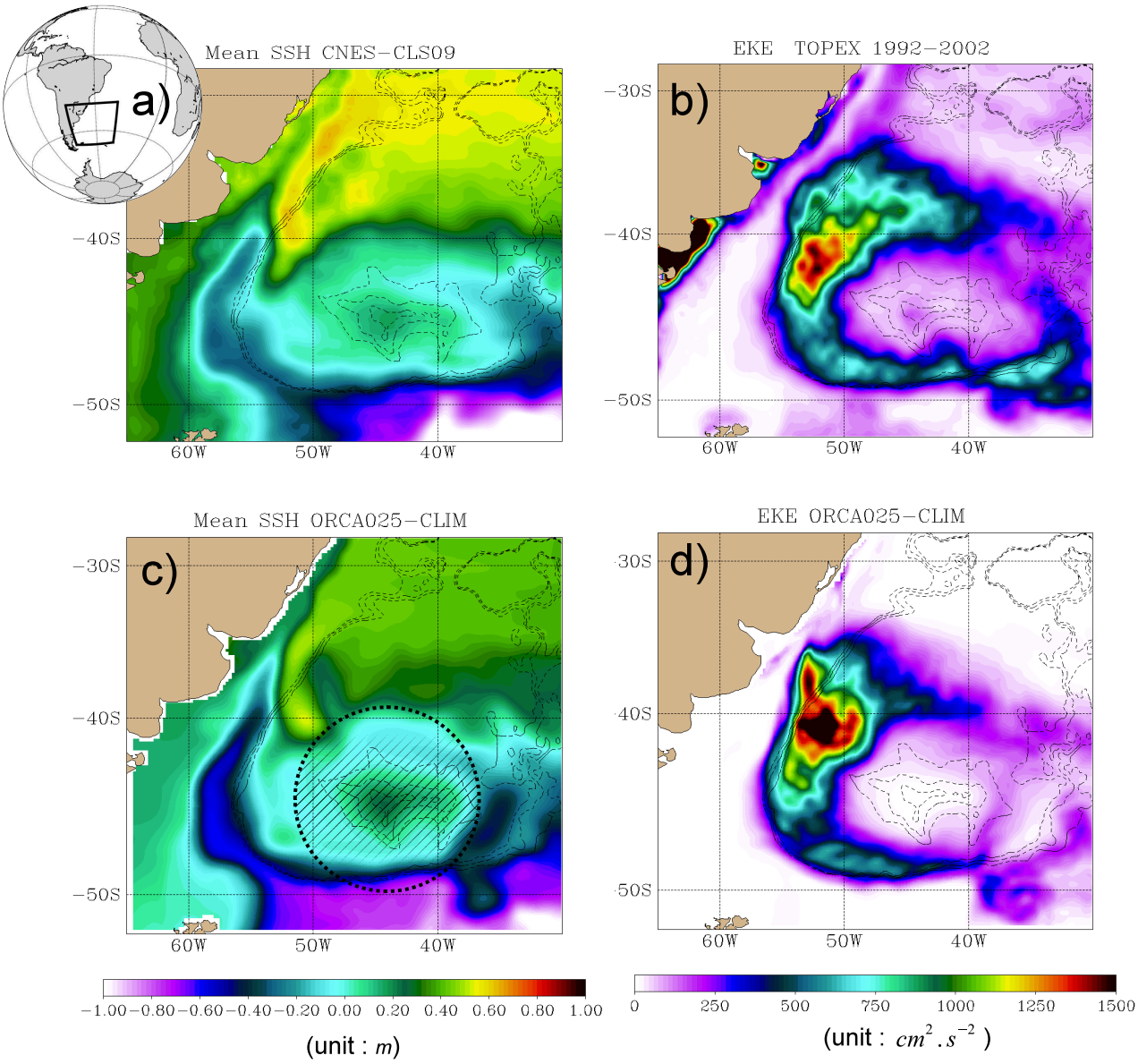

FIG. 2: **The Zapiola anticyclone in the Argentine Basin. a)** Mean Dynamical Topography (SSH) from CNES-CLS09 dataset. Above the Zapiola drift, SSH is proportional (and opposite) to the transport streamfunction since the flow is mostly depth independent. **b)** Surface eddy kinetic energy estimated from TOPEX altimeter over 1992-2002. **c,d)** Same quantities as a,b) in the model output over the last 10 years of the simulation. Isolines of f/h, where h is the local depth, are represented in thin dashed black line. The shaded circle in the lower left panel shows the region over which the diagnostics have been performed.

The formation of robust eddy-driven vortices above topography anomalies may provide an effective route for energy dissipation in the ocean. Indeed, because of the unstable nature of large scale oceanic flows, mesoscale eddies are ubiquitous in the ocean. In particular, high values of mesoscale eddy kinetic energy are observed along western boundaries of ocean basins. Here, we have depicted a situation where the mesoscale eddy kinetic energy can be absorbed above some topography anomaly (the Zapiola drift) and transferred to mean kinetic energy (the Zapiola anticyclone). The energy transfer is associated with the excitation, and the propagation of topographic Rossby waves [10]. Eventually, the mean kinetic energy of the anticyclone is dissipated through bottom friction. A simple estimation of the order of magnitude for this dissipation rate in the case of the Zapiola anticyclone gives a value of about 1. 10^{-3} W.m^{-2} over an area $A \sim 1.\ 10^6$ km^2, which amounts to a total of 1.10^{-3} TW. This amounts to a significant fraction (about one tenth) of the total sink of ocean-eddy energy at the western

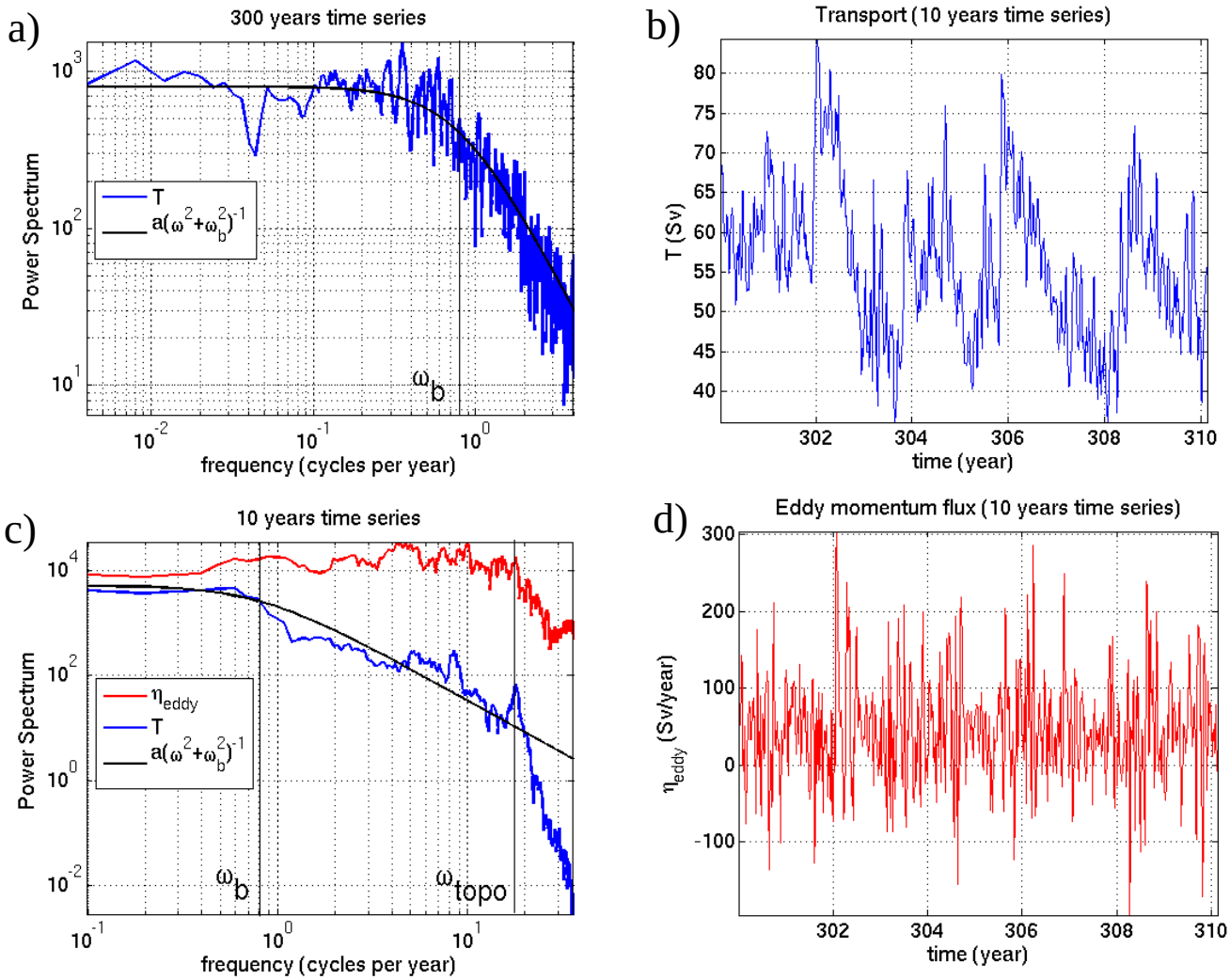

FIG. 3: **Transport fluctuations. a)** Transport power-spectrum $|\widetilde{\mathcal{T}}|^2(\omega)$ from the 300 years time series of monthly mean model output. **b)** Transport time series $\mathcal{T}(t)$ over the last 10 years time series from 5 days mean model output **c)** Transport and eddy momentum flux power-spectrum from the 10 years time series of 5 days mean model output. **d)** Eddy momentum flux time series from the 10 years time series of 5 days mean model output.

boundary of the South Atlantic [30]. Given the simple ingredients involved in setting the eddy-driven flow presented above, one might conjecture that the mechanism described in this letter could play an significant role in the internal low frequency dynamics and energetics of large scale oceanic currents.

Methods

A. Transport dynamics in a simple configuration.

Let us consider a barotropic (depth independent) flow above an axisymmetric topographic bump such that the total fluid depth $h(r)$ is increasing for $r < L_h$, and constant for $r > L_h$, see figure 1. We assume the existence of a stirring region outside the topography anomaly, but no other forcing mechanism. Above the topography anomaly (i.e. for $r < L_h$), the dynamics is governed by material advection of potential vorticity with a dissipation term $-\omega_b\zeta$ associated with a linear Ekman drag [24]:

$$\partial_t q + \mathbf{u}\nabla q = -\omega_b \frac{\zeta}{h} \ , \quad \nabla\left(h\mathbf{u}\right) = 0 \ , \quad q = \frac{\zeta + f}{h} \ , \quad (2)$$

where $\zeta = (\nabla \times \mathbf{u}) \cdot \mathbf{e}_z$ is the relative vorticity and f is the planetary vorticity taken here as a constant. $\mathbf{e}_z$ is a unit vector pointing upward.

We call v and u the radial and azimuthal velocities respectively (v is positive when directed outside the topography anomaly, u is positive when anti-clockwise). Defining eddies as deviation from the azimuthal average $u' = u - \overline{u}$ and integrating equation (2) inside a circle of constant r yields

$$\frac{\partial}{\partial t}\overline{u} = -\frac{1}{r^2}\frac{\partial}{\partial r}\left(r^2\overline{u'v'}\right) - \omega_b\overline{u}. \quad (3)$$

Multiplying equation (3) by the total fluid depth $h(r)$ and integrating from the center $r = 0$ to the boundary $r = L_h$ of the topography anomaly yields the transport equation (1) $\partial_t \mathcal{T} = \eta_{eddy} - \omega_b \mathcal{T}$, with $\mathcal{T} = \int_0^{L_h} \mathrm{d}r\ h\overline{u}$ and

$$\eta_{eddy} = -h\,\overline{v'u'}|_{r=L_h} + \int_0^{L_h} \mathrm{d}r\ \overline{v'u'} r^2 \frac{\partial}{\partial r}\left(\frac{h}{r^2}\right) . \quad (4)$$

Assuming that the typical variations of h over L_h are smaller than h, and that $|\overline{u'v'}/r| \ll |\partial_r \overline{u'v'}|$ (which corresponds to the limit case of a channel), the second term of the right hand side of (4) can be neglected, and $\eta_{eddy} \approx -h\,\overline{v'u'}|_{r=L_h}$ is then given by the eddy momentum fluxes at the boundary of the bump. The latter expression is used for diagnosing η_{eddy} with model output.

B. Ocean model configuration.

The ocean model results presented in this letter have been produced with the global eddy admitting DRAKKAR model configuration [1, 8]. This model configuration is based on the NEMO ocean/sea-ice modeling framework [18]. The model grid uses z-coordinates with 46 levels and a partial step representation of bottom topography. The model horizontal resolution at the equator is 1/4th degree and varies with the cosine of the latitude so that at 45°S the horizontal resolution is about $20km$. The model configuration uses a biharmonic viscosity for momentum and an isoneutral harmonic diffusivity for tracers. The bottom friction is a quadratic function of the bottom velocity $\mathbf{u_b}$ so that the bottom stress τ_b is given by

$$\tau_b = C_d \left(\mathbf{u_b}^2 + e\right)^{1/2} \mathbf{u_b},$$

where $e = 2.5\ 10^{-3}$ m^2.s^{-2} is the bottom turbulent kinetic energy due to tides and other small scale processes. According to common practice, the coefficient C_d is calibrated such that for weak barotropic flows, the bottom friction time-scale ω_b^{-1} is about 30 months. For a barotropic flow of about 0.1m.s^{-1} as the Zapiola anticyclone, the bottom friction time-scale ω_b^{-1} is about 14 months.

The model forcing used in the experiment is a repeated-year forcing build from the DRAKKAR forcing set DFS4 [3]. The forcing was built by computing a daily climatology of the variables available in DFS4 during 50 years at 6-hourly periods. Notably, the quadratic quantities (wind stress and bulk exchange coefficients) were also averaged in order to guarantee that the climatological forcing is energetically consistent [19]. The resulting forcing fields were then low-passed filtered in time (3-point hanning filter) to remove the remaining high-frequency noise. The resulting one year long forcing was applied repeatedly during the 310 years of the simulation.

C. Diagnostics.

The transport streamfunction ψ is defined according to $h\mathbf{u} = \mathbf{e}_z \times \nabla\psi$, where $\mathbf{u}$ is the depth averaged velocity. The transport is defined as the difference $\mathcal{T} = \overline{\psi}(boundary) - \psi(center)$, where $\psi(center)$ is the value of the streamfunction above the Zapiola drift ($45E45S$), and $\overline{\psi}(boundary)$ is the average of the streamfunction along the circle of radius $L_h = 600\ km$ depicted in figure 2-c.

The term η_{eddy} is estimated by computing the term $\overline{h}\overline{uv}$, with azimuthal averages taken along the same circle $r = L_h$. Output data of the 310 years simulation are monthly averaged, except for the last ten years of the simulation, where 5-days averages have been computed. Eddy terms can therefore only be computed over the last 10 years.

Importantly, the eddy term $\overline{v'u'}$ computed as an azimuthal average is well defined for a given time (although not associated with a single spatial point). By contrast and according to common practice [29], the maps of eddy kinetic energy presented figures 2-a,b are obtained by computing variance from time series at each point.

Acknowledgments

The model simulation discussed herein was performed at CINES (Montpellier, France) as part of the "Grands Challenges GENCI/CINES 2008" and benefited from the technical expertise of Nicole Audiffren. JLS, JMM and BB are supported by the CNRS. AV was supported by DoE grant DE-SC0005189 and NOAA grant NA08OAR4320752 during part of this work. We thank Isaac Held for suggesting the analogy with the atmosphere. The diagnostic presented in this letter are inspired from a poster presented by Chris W. Hughes at the European Geophysical Union General Assembly 2008 under reference EGU2008-A-06866.

[1] Barnier, B. *et al.* Impact of partial steps and momentum advection schemes in a global ocean circulation model at eddy-permitting resolution. *Ocean Dynamics*, 56:543–567, December 2006.

[2] Berloff, P. S., and McWilliams, J. C. Large-Scale, Low-Frequency Variability in Wind-Driven Ocean Gyres. *Journal of Physical Oceanography*, 29:1925–1949, August 1999.

[3] Brodeau, L. *et al.* An ERA40 based atmospheric forcing for global ocean circulation models. *Oc. Model.*, 31:88–104, 2009.

[4] Cane, M. A. Climate science: Decadal predictions in

demand. *Nature Geoscience*, 3:231–232, April 2010.

[5] de Miranda, A. P., Barnier, B., and Dewar, W.K. On the dynamics of the Zapiola Anticyclone. *J. Geophys. Res.*, 104:21137 – 21150, September 1999.

[6] Dewar, W.K. Topography and barotropic transport control by bottom friction. *J. Mar. Res.*, 56:295–328, 1998.

[7] Dijkstra,H. A., and Ghil, M. Low-frequency variability of the large-scale ocean circulation: A dynamical systems approach. *Reviews of Geophysics*, 43:3002, September 2005.

[8] The Drakkar Group. Eddy permitting ocean circulation hindcasts of past decades. *Clivar Exchanges*, 42:8–10, 2007.

[9] Frankignoul, C., Müller, P., and Zorita, E. A Simple Model of the Decadal Response of the Ocean to Stochastic Wind Forcing. *Journal of Physical Oceanography*, 27:1533–1546, August 1997.

[10] Fu, L.-L. Interaction of Mesoscale Variability with Large-Scale Waves in the Argentine Basin. *Journal of Physical Oceanography*, 37:787, 2007.

[11] Fu, L.-L., Cheng, B. , and Qiu, B. 25-Day Period Large-Scale Oscillations in the Argentine Basin Revealed by the TOPEX/Poseidon Altimeter. *Journal of Physical Oceanography*, 31:506–517, February 2001.

[12] Ghil, M. *et al.* Advanced Spectral Methods for Climatic Time Series. *Reviews of Geophysics*, 40:1003, September 2002.

[13] Hasselmann, K. Stochastic climate models, Part I, Theory. *Tellus*, 28:473, 1976.

[14] Held, I. M. Momentum transport by quasi-geostrophic eddies. *Journal of Atmospheric Sciences*, 32:1494–1496, July 1975.

[15] Hogg, A. M., Killworth, P. D., Blundell, J. R., and Dewar, W. K. Mechanisms of Decadal Variability of the Wind-Driven Ocean Circulation. *Journal of Physical Oceanography*, 35:512, 2005.

[16] Hughes, C. W., Stepanov, V. N., Fu, L.-L., Barnier, B., and Hargreaves, G. W. Three forms of variability in Argentine Basin ocean bottom pressure. *Journal of Geophysical Research (Oceans)*, 112:1011, January 2007.

[17] Lorenz, D. J., and Hartmann, D. L. Eddy-Zonal Flow Feedback in the Southern Hemisphere. *Journal of Atmospheric Sciences*, 58:3312–3327, November 2001.

[18] Madec, G. Nemo ocean engine. *Note du Pole de modelisation, Institut Pierre-Simon Laplace (IPSL), France*, 27:ISSN 1288–1619, 2008.

[19] Penduff, T. *et al.* Sea-level expression of intrinsic and forced ocean variabilities at interannual time scales. *"Journal of Climate"*, in revision.

[20] Rhines, P. , and Young, W.R. Homogenization of potential vorticity in planetary gyres. *Journal of Fluid Mechanics*, 122:347–367, 1982.

[21] Saraceno, M. , Provost, C., and Zajaczkovski,U. Long-term variation in the anticyclonic ocean circulation over the Zapiola Rise as observed by satellite altimetry: Evidence of possible collapses. *Deep Sea Research Part I: Oceanographic Research*, 56:1077–1092, July 2009.

[22] Saunders, P. M., and King, B. A. Oceanic Fluxes on the WOCE A11 Section. *J. Phys. Oceanogr.*, 25:1942–1958, September 1995.

[23] Simonnet, E., Ghil, M., and Dijkstra, H. Homoclinic bifurcations in the quasi-geostrophic double-gyre circulation. *J. Mar. Res.*, 63:931–956, 2005.

[24] Vallis, G. K. *Atmospheric and Oceanic Fluid Dynamics.* November 2006.

[25] Volkov, D. L., and Fu, L.-L. The role of vorticity fluxes in the dynamics of the Zapiola Anticyclone. *J. Geophys. Res.*, 113, 2008.

[26] von Storch, H., and Zwiers, F. W. *Statistical Analysis in Climate Research.* March 2002.

[27] Weatherly, G. On deep-current and hydrographic observations from a mudwave region and elsewhere in the Argentine Basin. *Deep Sea Res. Part II: Topical Studies in Oceanography*, 40:939–961, 1993.

[28] Weijer, W., Vivier, F., Gille, S. T., and Dijkstra, H. A. Multiple Oscillatory Modes of the Argentine Basin. Part I: Statistical Analysis. *Journal of Physical Oceanography*, 37:2855, 2007.

[29] Williams, R. G., Wilson, C., and Hughes, C. W. Ocean and Atmosphere Storm Tracks: The Role of Eddy Vorticity Forcing. *Journal of Physical Oceanography*, 37:2267, 2007.

[30] Zhai, X., Johnson, H. L., and Marshall, D. P. Significant sink of ocean-eddy energy near western boundaries. *Nature Geoscience*, 3:608–612, September 2010.